



Quantum oscillation in carrier transport in two-dimensional junctions

Journal:	<i>Nanoscale</i>
Manuscript ID	NR-COM-02-2018-001359.R1
Article Type:	Communication
Date Submitted by the Author:	19-Mar-2018
Complete List of Authors:	Zhang, Junfeng; Shanxi Normal University, School of Physics and Information Engineering Xie, Weiyu; Rensselaer Polytechnic Institute Agiorgousis, Michael; Rensselaer Polytechnic Institute, Department of Physics, Applied Physics, and Astronomy Choe, Duk-hyun; Rensselaer Polytechnic Institute Meunier, Vincent; Rensselaer Polytechnic Institute, Department of Physics, Applied Physics, and Astronomy Xu, Xiaohong; Shanxi Normal University, School of Chemistry and Materials Science Zhao, Jijun; Dalian Institute of Technology, College of Advanced Science and Technology Zhang, Shengbai; Rensselaer Polytechnic Institute,



Journal Name

COMMUNICATION

Quantum oscillation in carrier transport in two-dimensional junctions

Received 00th January 20xx,
Accepted 00th January 20xx

Junfeng Zhang^a, Weiyu Xie^b, Michael L. Agiorgousis^b, Duk-Hyun Choe^b, Vincent Meunier^b, Xiaohong Xu^a, Jijun Zhao^{*c}, and Shengbai Zhang^{*b}

DOI: 10.1039/x0xx00000x

www.rsc.org/

Two-dimensional (2D) junction devices have recently attracted considerable attention. Here, we show that most 2D junction structures, regardless vertical or lateral, act as a lateral monolayer-bilayer-monolayer junction in their operation. In particular, a vertical structure cannot function as a vertical junction as having been widely believed in the literature. Due to a larger electrostatic screening, the bilayer region in the junction always has a smaller band gap than its monolayer counterpart. As a result, a potential well, aside from the usual potential barrier, will form universally in the bilayer region to affect the hole or electron quantum transport in the form of transmission or reflection. Taking black phosphorus as an example, our calculations using non-equilibrium Green function combined with density functional theory show a distinct oscillation in the transmission coefficient in a two-electrode prototypical device, and the results can be qualitatively understood using a simple quantum well model.

Two-dimensional (2D) materials have unique properties and hold great promise for novel applications. One important area is in the electronic device where significant effort has been made to integrate different 2D materials into vertical or lateral junctions, as a basic component of nanodevices such as field-effect transistor (FET), *p-n* diode, and photodiode. The vertical and lateral junctions using 2D materials such as graphene, *h*-BN, black phosphorous (BP), and transition metal dichalcogenides (TMDs), have been fabricated in laboratory¹⁻⁸.

However, in practical applications, most of 2D junctions are neither pure vertical nor pure lateral as often assumed in theory^{9, 10}, but a monolayer-bilayer-monolayer (ML-BL-ML) structure. In experiment, it is difficult to make an electrode contact to only one ML without metallization between the electrode and the entire 2D stack. Even if such a contact can be made, one cannot avoid current tunneling between the layers¹¹⁻¹⁸. Hence, most realistic 2D vertical junctions follow the schematic plot shown in Figure 1a, where the overall structure can be viewed as a three-junction device with one vertical and two lateral junctions in series. It is therefore not surprising that an intended vertical *p-n* junction may not behave as a vertical diode but rather as lateral one^{15, 17}. For the 2D lateral junctions fabricated by the two-step chemical vapor deposition (CVD) method¹⁹⁻²⁴, it is also frequent to obtain structures with partial overlap of the MLs to form a common BL region at the interface, especially when the component materials have a large lattice mismatch²⁵⁻²⁷. In some of the recent van der Waals 2D junctions²⁸⁻³⁰, graphene has been used as part of the electrodes for lower contact resistance. This, however, does not change the fact that the device is always a multi-junction device, as we will discuss below.

We can define the ratio of the BL region over the ML regions (which for simplicity is assumed to be symmetric, see Figure 1a) as $R_{B/M} = L_{BL}/L_{ML}$, in which L_{BL} and L_{ML} are the lengths of the BL and ML regions, respectively. With such a definition, a vertical junction may be classified as a special case of lateral junctions when $R_{B/M} \rightarrow \infty$. Even in this case, the two lateral junctions to the electrodes cannot be ignored. It is thus clear that the fundamental device physics of 2D junctions such as the band offsets and associated transport properties can deviate significantly from those predicted for either pure vertical or pure lateral structures.

^a Research Institute of Materials Science of Shanxi Normal University & Collaborative Innovation Center for Shanxi Advanced Permanent Magnetic Materials and Technology, Linfen 041004, China.

^b Department of Physics, Applied Physics, and Astronomy, Rensselaer Polytechnic Institute, Troy, NY 12180, USA. Email: zhangs9@rpi.edu

^c Key Laboratory of Materials Modification by Laser, Ion and Electron Beams (Dalian University of Technology), Ministry of Education, Dalian 116024, China. Email: zhaojj@dlut.edu.cn

† Footnotes relating to the title and/or authors should appear here.

Electronic Supplementary Information (ESI) available: The LDOS maps of the stacked and staggered structures with $L_{BL} \sim 3$ nm (Figure S1). The maximum and minimum transmission coefficients from the symmetric and asymmetric QW models, respectively (Figure S2). Details on the quantum-well model. See DOI: 10.1039/x0xx00000x

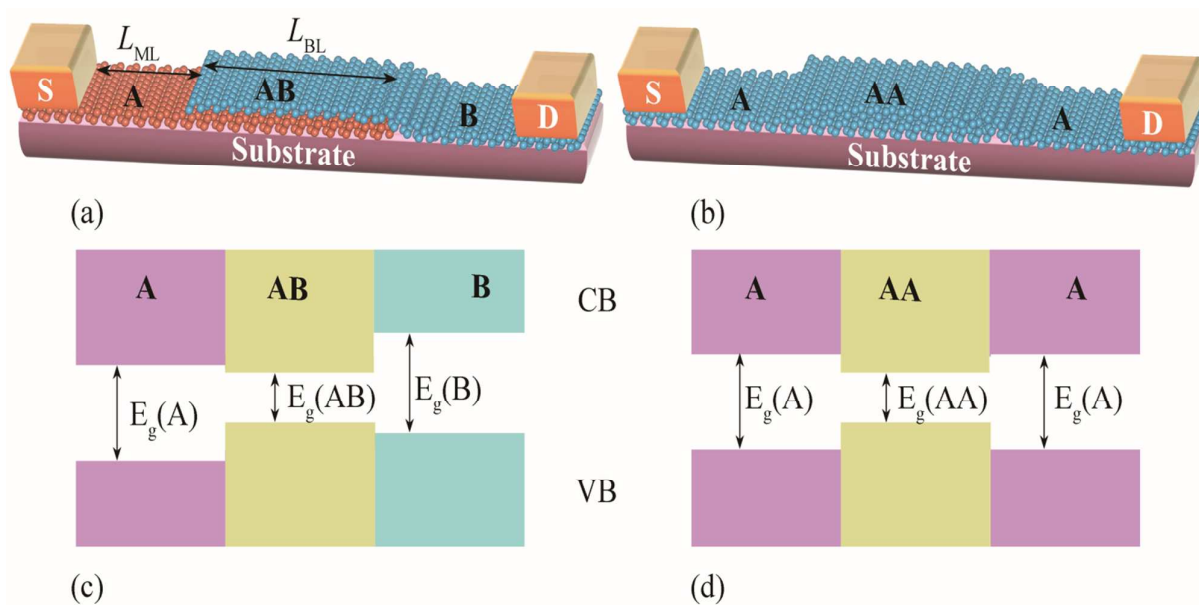


Fig. 1 Typical structures of two-electrode devices with (a) an asymmetric (A-AB-B) and (b) a symmetric (A-AA-A) 2D junction. S and D stand for source and drain electrodes. (c) and (d) are the corresponding schematic band alignments. CB and VB stand for conduction band and valence band, respectively.

Figures 1a-b show two prototypical 2D junctions with either two components^{26, 27, 31, 32} (heterojunction between A and B, i.e., A-AB-B) or single component^{33, 34} (homojunction between A and A, i.e., A-AA-A). An important property of 2D semiconductors is that a BL or few-layer structure always has a smaller band gap than the ML system. As a result, a potential well naturally forms in the BL region for either electron or hole carriers, as schematically shown in Figures 1c-d. In the conventional 3D superlattices, the effects of quantum well (QW) have been extensively studied^{35, 36}. In contrast, QW effects on the carrier transport in 2D junctions have attracted little attention.

In this communication, by a combined non-equilibrium Green function (NEGF) and density functional theory (DFT) calculation of model 2D junction devices, we show a universal oscillation in the low-energy carrier transmission due to the presence of QW. We take black phosphorus (BP) as an example for it is an elemental semiconductor with a high carrier mobility (up to $1,000 \text{ cm}^2 \text{ V}^{-1} \text{ s}^{-1}$)^{37, 38} and a large band gap dependent on layer thickness^{38, 39}. The oscillation in the transmission coefficient from NEGF-DFT calculations can be understood by a one-dimensional (1D) QW model. Both theories suggest that the length of QW, which may vary from atomic scale to the mean free path of electrons (e.g., $\sim 10 \text{ nm}$ in graphene and TMD materials^{40, 41}), is critical to the quantum conductance of 2D junction devices.

We start from DFT calculations for the A-AA-A BP homojunction, while the particular choice of systems should not affect the generality of our findings. Supercells of 2D BP junctions were constructed by joining ML and AB-stacked BL nanoribbons at zigzag interfaces, as shown in Figure 2a. We

used a large supercell of 8.27 nm (18 unit cells) in lateral to ensure a reasonably good bulk band structure in the centers of both ML and BL regions. The dangling bonds at the BL edges

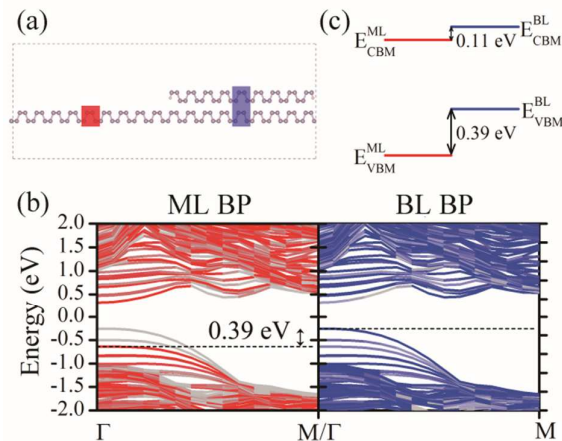


Fig. 2 (a) Structural model of 2D BP homojunction used in the DFT calculation. Shaded red and blue squares denote the central unit cells in the ML and BL domains, respectively. (b) Band structure of a 2D BP homojunction with zigzag edges. We performed atomic projection onto the red and blue central unit cells in (a): states with 10% projection in the ML red square are shown in red, BL states with 10% projection in the BL blue square are shown in blue, and those with less than 10% projections are shown in grey. (c) Band alignment in 2D BP homojunction determined from the band structures in (b). A 0.39 eV valence band offset between the ML and BL regions is calculated from PBE functional.

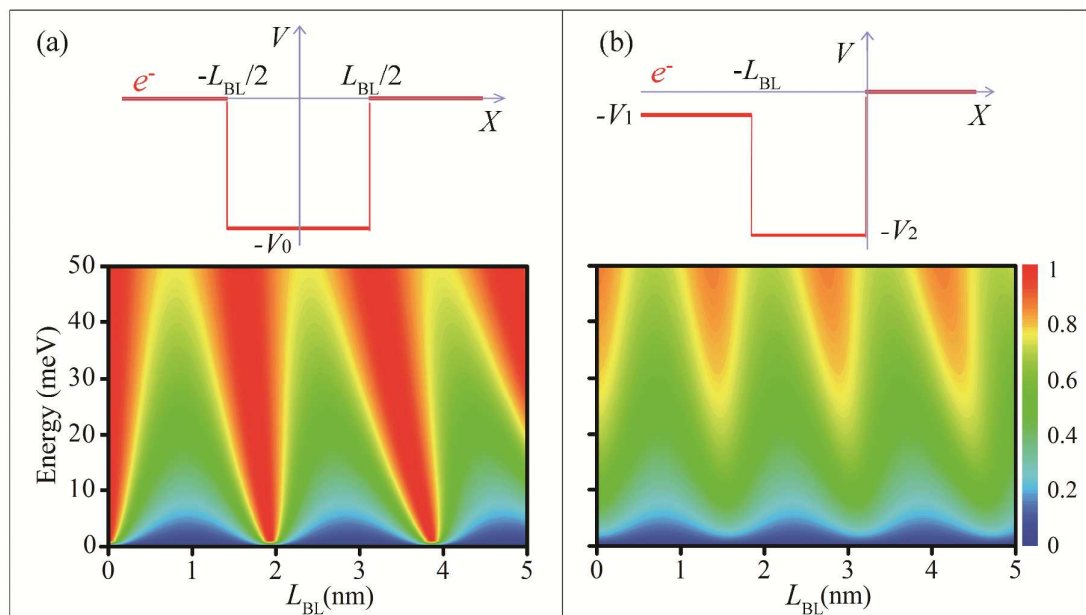


Fig. 3 Schematic plots of the quantum well models (upper panel) and the corresponding transmission coefficients (lower panel) for (a) symmetric (A/AA/A) and (b) asymmetric (A/AB/B) 2D homojunctions. In (a), the well depth V_0 is set at 0.1 eV. In (b), however, the depths are $V_1 = 0.05$ and $V_2 = 0.15$ eV.

were passivated by hydrogen atoms. A vacuum space of 3 nm thickness in the direction perpendicular to the BP basal plane was added to avoid spurious interactions between periodic images. The atomic structures and electronic properties were calculated using DFT and the projector-augmented wave (PAW) method⁴², as implemented in the Vienna *ab initio* simulation package (VASP)^{43, 44}. The Perdew–Burke–Ernzerhof (PBE)⁴⁵ functional was used to describe the exchange–correlation interactions. The planewave basis was expanded to 400 eV. The Brillouin zones were sampled by \mathbf{k} point grids with a uniform separation of 0.015 \AA^{-1} .

When the lateral length is sufficiently big, the behavior of a 2D junction should obey the Anderson limit⁹. Hence, here we consider a 2D homojunction of shorter length, i.e., 10 nm supercell length. From DFT calculations of the combined ML–BL BP system, the band gaps in the bulk ML and BL regions are 0.97 and 0.69 eV (see Figure 2b), respectively, compared to the values of 0.88 and 0.59 eV for bulk ML and BL BPs^{46, 47}. In accordance, the valence and conductance band offsets of the 2D homojunction are 0.39 and 0.11 eV, as displayed in Figure 2c. Here we focus on the former (corresponding to hole transport), as a larger band offset could make it easier to observe the QW effect.

One can understand the QW effect on transport by quantum mechanics for a single particle, where the potential $v(x)$ is $-V_0$ inside the well and zero outside. Using the boundary conditions, the transmission coefficient (T) of a carrier can be readily derived as⁴⁸:

$$T = \left[1 + \frac{V_0^2}{4E(E+V_0)} \cdot \sin^2 \left(\frac{L_{\text{BL}}}{\hbar} \sqrt{2m(E+V_0)} \right) \right]^{-1} \quad (1)$$

where L_{BL} is the length of the potential well, m is the carrier effective mass, and E is the energy of carrier. With a fixed V_0 , the calculated T is given in Figure 3a (lower panel), showing a sinusoidal oscillation with respect to L_{BL} . At a low energy, e.g., $E < 50$ meV, T oscillates quickly between 0 and 1. However, when the energy is higher, T approaches a constant of 1, irrespective of L_{BL} . Most strikingly, low-energy carriers could be totally blocked ($T = 0$, OFF state) or transmitted ($T = 1$, ON state) depending on the choice of L_{BL} .

To verify the prediction by such a simple quantum mechanics model, we constructed model devices with two electrodes, either placed in the same ML or in different MLs, as shown in Figures 4. We adopted Au electrodes as source and drain for their good electrical conductivity. The quantum transmission coefficients were calculated by including self-energies for the coupling of scattering region to the semi-infinite Au leads under zero bias voltage. Real space linear combination of DZP atomic orbital basis was employed. The cutoff energy for the real space grid was set to 400 eV. A $1 \times 21 \times 1$ \mathbf{k} point mesh was employed in the Brillouin zone integration for transport calculations.

We perform a series of NEGF calculations on two-electrode devices made of 2D BP homojunctions. Two examples are considered: stacked (Figure 4a) and staggered (Figure 4b) junctions, where the dangling edges are passivated by hydrogen atoms. In either case, a potential well is formed in the BL region for holes. The difference between the two models is that the transmitted electrons in the staggered junction must participate in a vertical interlayer transport. The

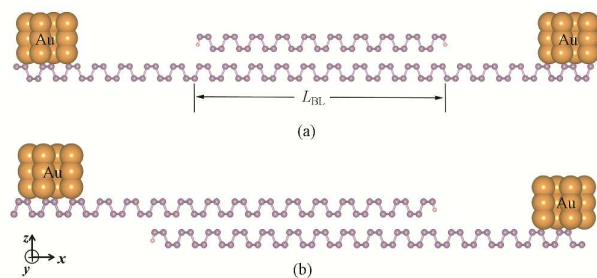


Fig. 4 Structure models of (a) stacked and (b) staggered 2D BP homojunction used in the NEGF calculations. L_{BL} stands for the length of the bilayer region.

transport properties are obtained with a fixed scattering region length (~ 9 nm) but a varying L_{BL} from 1.1 to 4.5 nm.

Figure S1 of ESI shows, as an example for $L_{BL} \sim 3$ nm, the LDOS in the scattering region in stacked and staggered 2D BP junctions. Metallic behaviour can be readily seen in both $x < 1$ nm and > 8 nm regions of the BPs, suggesting a buffer-region effect from the metal electrodes. Consistent with the DFT results in Figure 2b, the valence band maximum (VBM) of the BL region acts as a potential well (as labelled by dashed lines in Figure S1). It is noteworthy that the shape of potential well deviates from that of the ideal square well model due to the relaxation of charge at interface.

Figure 5 shows transmission coefficients for both homojunctions with $L_{BL} = 1 - 4.5$ nm. In our calculation, the system is periodic along the interface (i.e., y direction), resulting in a band dispersion. Hence, the depth of the potential well varies with \mathbf{k} points as shown in Figure 2b. For example, the well depth is 390 meV at Γ , but only 70 meV at M. Consequently, carriers with different momenta would experience wells at different depths. For simplicity, we consider Γ point scattering only, as holes are mostly localized here. An oscillating behaviour can be clearly seen in Figure 5 for both stacked and staggered junctions. For comparison, results of the QW model in Eq. (1) are also given, which qualitatively agree with NEGF results and display an oscillation with L_{BL} . Despite some deviations from the QW model due to its oversimplification nature, it captures the essential physics well. Previously, such kind of quantum oscillation in transport behaviour were observed in 1D heterojunctions of carbon nanotubes⁴⁹ and 3D Bi₂Se₃ superlattices³⁵ and were attributed to the resonant cavity-like interference phenomena in the contact region.

Note that the existence of a potential well is not limited to BP or a homojunction, but should be more general for most of 2D junctions. For a 2D heterojunction (A-AB-B, see Figure 1b) with type I or II band alignment with moderate band offset between A and B, the symmetric potential well will be replaced by an asymmetric one, as shown in Figure 3b. The QW model predicts that (see details in ESI)

$$T = \frac{16k_1k_2^2k_3}{k_2^2(k_1+k_2)^2 + (k_2^2 - k_1^2)(k_2^2 - k_3^2)\sin^2 k_2 a} \times \frac{k_2k_3}{(k_2+k_3)^2} \quad (2)$$

in which $k_1 = \sqrt{2m(E+V_1)}/\hbar$, $k_2 = \sqrt{2m(E+V_2)}/\hbar$, $k_3 = \sqrt{2mE}/\hbar$, where m , \hbar , L_{BL} , and E are already defined in Eq. (1), V_1 is the band offset

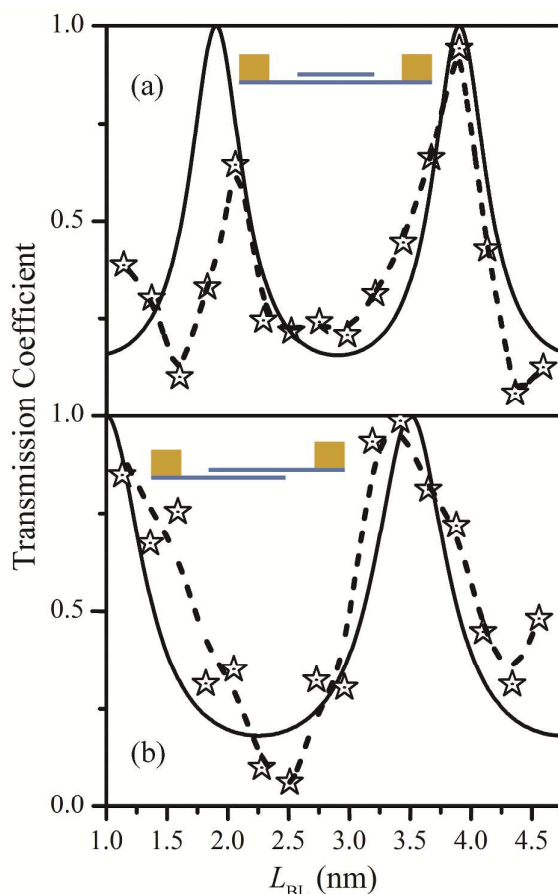


Fig. 5 Transmission coefficients of the quantum-well model (black lines) and the NEGF-DFT calculations (stars) for (a) stacked and (b) staggered BP junctions. Insets show the schematic models for transport calculations. Dashed lines linking the stars are drawn to guide eyes. Transmission coefficients in DFT-NEGF calculations were taken from the carriers with energy 160 meV. In the model calculation, kinetic energy of the carriers and the well depth were set to 80 and 4 meV in (a), and 57 and 3 meV in (b), respectively.

between material A and B, and $(V_2 - V_1)$ is the potential well indicated in Figure 3b. If $A = B$, V_1 vanishes and $(V_2 - V_1)$ becomes V_0 in Eq. (1). Similar to the homo case, the oscillatory behavior of T is also evident in Figure 3b (the lower panel with $V_1 = 0.05$ eV and $V_2 = 0.15$ eV). Different from the homo case, however, the maximum transmission coefficient here can hardly approach 1 when E is small, as also indicated in Figure S2 of ESI. As long as the BL region has a smaller band gap than the ML region, an oscillation in T exists. In general, quantum oscillation may occur in a 2D device provided that the band gap of the 2D material is spatially inhomogeneously tuned. The exceptions occur if the carrier transport is non-ballistic (i.e., when the scattering region is larger than the mean free path of the carriers) or the energy of the carriers is too high so that the effect of the quantum well diminishes. For 2D materials, such as graphene⁵⁰ and TMD materials^{40, 51}, the mean free paths are ~ 10 nm. Then, the oscillation in transmission coefficient may

be observable when the bilayer region is narrower than 10 nm. The controllable QW effect revealed here provides a novel route in designing ultra-high ON/OFF ratio transport devices.

To summarize, our analysis suggests that most of the 2D junctions experimentally realizable today are neither a purely vertical junction nor a purely lateral junction, but take the hybrid ML-BL-ML form. Our NEGF-DFT calculations combined with analytical quantum mechanics models, unveil the unexpected roles of the BL region. Rather than functioning as a vertical junction as often believed, the BL acts as a quantum well to result in quantum oscillations in the transmission. Both the magnitude and period of the oscillations are strong functions of the width of the BL region so they should be detectable and controllable in experiment. The presence of the quantum well oscillations is vital to 2D device design.

Conflicts of interest

There are no conflicts to declare.

Acknowledgements

JFZ was supported by the National Natural Science Foundation of China (11304191), the Natural Science Foundation of Shanxi province (2015021011) and CSC Award No. 201608140024. WYX was supported by the US-NSF under Award No. 1104786 and SBZ was supported by the US-DOE under Grant No. DESC0002623. The supercomputer time by NERSC under DOE contract No. DE-AC02-05CH11231 and by the CCI at RPI are acknowledged.

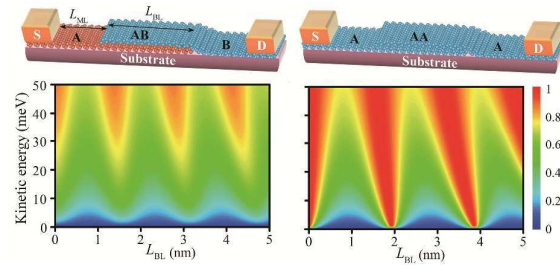
References

- 1 A. K. Geim and I. V. Grigorieva, *Nature*, 2013, **499**, 419-425.
- 2 H. Lim, S. I. Yoon, G. Kim, A.-R. Jang and H. S. Shin, *Chem Mater*, 2014, **26**, 4891-4903.
- 3 H. Wang, F. Liu, W. Fu, Z. Fang, W. Zhou and Z. Liu, *Nanoscale*, 2014, **6**, 12250-12272.
- 4 Y. Liu, N. O. Weiss, X. Duan, H.-C. Cheng, Y. Huang and X. Duan, *Nature Rev Mater*, 2016, **1**, 16042.
- 5 A. Pant, Z. Mutlu, D. Wickramaratne, H. Cai, R. K. Lake, C. Ozkan and S. Tongay, *Nanoscale*, 2016, **8**, 3870-3887.
- 6 D. Li, M. Chen, Z. Sun, P. Yu, Z. Liu, P. M. Ajayan and Z. Zhang, *Nature Nanotechnol*, 2017, **12**, 901-906.
- 7 J. Zhao, K. Cheng, N. Han and J. Zhang, *WIREs Comput Mol Sci*, 2017, DOI: 10.1002/wcms.1353, e1353.
- 8 Z. Cai, B. Liu, X. Zou and H.-M. Cheng, *Chem Rev*, 2018, DOI: 10.1021/acs.chemrev.7b00536.
- 9 J. Zhang, W. Xie, J. Zhao and S. Zhang, *2D Mater*, 2017, **4**, 015038.
- 10 H. Yu, A. Kutana and B. I. Yakobson, *Nano Lett*, 2016, **16**, 5032-5036.
- 11 T. Roy, M. Tosun, X. Cao, H. Fang, D.-H. Lien, P. Zhao, Y.-Z. Chen, Y.-L. Chueh, J. Guo and A. Javey, *ACS Nano*, 2015, **9**, 2071-2079.
- 12 S. Chuang, R. Kapadia, H. Fang, T. C. Chang, W.-C. Yen, Y.-L. Chueh and A. Javey, *Appl Phys Lett*, 2013, **102**, 242101.
- 13 M. M. Furchi, A. Pospischil, F. Libisch, J. Burgdörfer and T. Mueller, *Nano Lett*, 2014, **14**, 4785-4791.
- 14 Y. Deng, Z. Luo, N. J. Conrad, H. Liu, Y. Gong, S. Najmaei, P. M. Ajayan, J. Lou, X. Xu and P. D. Ye, *ACS Nano*, 2014, **8**, 8292-8299.
- 15 R. Cheng, D. Li, H. Zhou, C. Wang, A. Yin, S. Jiang, Y. Liu, Y. Chen, Y. Huang and X. Duan, *Nano Lett*, 2014, **14**, 5590-5597.
- 16 F. Wang, Z. Wang, K. Xu, F. Wang, Q. Wang, Y. Huang, L. Yin and J. He, *Nano Lett*, 2015, **15**, 7558-7566.
- 17 C.-H. Lee, G.-H. Lee, A. M. van der Zande, W. Chen, Y. Li, M. Han, X. Cui, G. Arefe, C. Nuckolls, T. F. Heinz, J. Guo, J. Hone and P. Kim, *Nature Nanotechnol*, 2014, **9**, 676-681.
- 18 M.-H. Doan, Y. Jin, S. Adhikari, S. Lee, J. Zhao, S. C. Lim and Y. H. Lee, *ACS Nano*, 2017, **11**, 3832-3840.
- 19 Q. Yu, L. A. Jauregui, W. Wu, R. Colby, J. Tian, Z. Su, H. Cao, Z. Liu, D. Pandey, D. Wei, T. F. Chung, P. Peng, N. P. Guisinger, E. A. Stach, J. Bao, S.-S. Pei and Y. P. Chen, *Nature Mater*, 2011, **10**, 443-449.
- 20 L. Liu, J. Park, D. A. Siegel, K. F. McCarty, K. W. Clark, W. Deng, L. Basile, J. C. Idrobo, A.-P. Li and G. Gu, *Science*, 2014, **343**, 163-167.
- 21 X. Duan, C. Wang, J. C. Shaw, R. Cheng, Y. Chen, H. Li, X. Wu, Y. Tang, Q. Zhang, A. Pan, J. Jiang, R. Yu, Y. Huang and X. Duan, *Nature Nanotechnol*, 2014, **9**, 1024-1030.
- 22 C. Huang, S. Wu, A. M. Sanchez, J. J. P. Peters, R. Beanland, J. S. Ross, P. Rivera, W. Yao, D. H. Cobden and X. Xu, *Nature Mater*, 2014, **13**, 1096-1101.
- 23 Y. Gong, J. Lin, X. Wang, G. Shi, S. Lei, Z. Lin, X. Zou, G. Ye, R. Vajtai, B. I. Yakobson, H. Terrones, M. Terrones, B. Tay, J. Lou, S. T. Pantelides, Z. Liu, W. Zhou and P. M. Ajayan, *Nature Mater*, 2014, **13**, 1135-1142.
- 24 X. Duan, C. Wang, J. C. Shaw, R. Cheng, Y. Chen, H. Li, X. Wu, Y. Tang, Q. Zhang, A. Pan, J. Jiang, R. Yu, Y. Huang and X. Duan, *Nature Nanotechnol*, 2014, **9**, 1024-1030.
- 25 Y. Gong, S. Lei, G. Ye, B. Li, Y. He, K. Keyshar, X. Zhang, Q. Wang, J. Lou, Z. Liu, R. Vajtai, W. Zhou and P. M. Ajayan, *Nano Lett*, 2015, **15**, 6135-6141.
- 26 M. H. D. Guimarães, H. Gao, Y. Han, K. Kang, S. Xie, C.-J. Kim, D. A. Muller, D. C. Ralph and J. Park, *ACS Nano*, 2016, **10**, 6392-6399.
- 27 X. Ling, Y. Lin, Q. Ma, Z. Wang, Y. Song, L. Yu, S. Huang, W. Fang, X. Zhang, A. L. Hsu, Y. Bie, Y.-H. Lee, Y. Zhu, L. Wu, J. Li, P. Jarillo-Herrero, M. Dresselhaus, T. Palacios and J. Kong, *Adv Mater*, 2016, **28**, 2322-2329.
- 28 A. Avsar, I. J. Vera-Marun, J. Y. Tan, K. Watanabe, T. Taniguchi, A. H. Castro Neto and B. Özyilmaz, *ACS Nano*, 2015, **9**, 4138-4145.
- 29 G.-H. Lee, X. Cui, Y. D. Kim, G. Arefe, X. Zhang, C.-H. Lee, F. Ye, K. Watanabe, T. Taniguchi, P. Kim and J. Hone, *ACS Nano*, 2015, **9**, 7019-7026.
- 30 T. Roy, M. Tosun, J. S. Kang, A. B. Sachid, S. B. Desai, M. Hettick, C. C. Hu and A. Javey, *ACS Nano*, 2014, **8**, 6259-6264.
- 31 R. Zhou, V. Ostwal and J. Appenzeller, *Nano Lett*, 2017, **17**, 4787-4792.
- 32 X. Liu, Z. Wei, I. Balla, A. J. Mannix, N. P. Guisinger, E. Luijten and M. C. Hersam, *Sci Adv*, 2017, **3**, e1602356.

COMMUNICATION

Journal Name

- 33 C. Zhang, Y. Chen, J.-K. Huang, X. Wu, L.-J. Li, W. Yao, J. Tersoff and C.-K. Shih, *Nature Commun*, 2016, **7**, 10349.
- 34 H.-F. Lin, L.-M. Liu and J. Zhao, *J Mater Chem C*, 2017, **5**, 2291-2300.
- 35 L. D. Hicks and M. S. Dresselhaus, *Phys Rev B*, 1993, **47**, 12727-12731.
- 36 Y.-H. Kuo, Y. K. Lee, Y. Ge, S. Ren, J. E. Roth, T. I. Kamins, D. A. B. Miller and J. S. Harris, *Nature*, 2005, **437**, 1334-1336.
- 37 L. Li, Y. Yu, G. J. Ye, Q. Ge, X. Ou, H. Wu, D. Feng, X. H. Chen and Y. Zhang, *Nature Nanotechnol*, 2014, **9**, 372-377.
- 38 J. Qiao, X. Kong, Z.-X. Hu, F. Yang and W. Ji, *Nature Commun*, 2014, **5**, 4475.
- 39 H. Liu, A. T. Neal, Z. Zhu, Z. Luo, X. Xu, D. Tománek and P. D. Ye, *ACS Nano*, 2014, **8**, 4033-4041.
- 40 Q. Cui, F. Ceballos, N. Kumar and H. Zhao, *ACS Nano*, 2014, **8**, 2970-2976.
- 41 J. Lu, L. C. Gomes, R. W. Nunes, A. H. Castro Neto and K. P. Loh, *Nano Lett*, 2014, **14**, 5133-5139.
- 42 G. Kresse and D. Joubert, *Phys Rev B*, 1999, **59**, 1758-1775.
- 43 G. Kresse and J. Furthmüller, *Comp Mater Sci*, 1996, **6**, 15-50.
- 44 G. Kresse and J. Furthmüller, *Phys Rev B*, 1996, **54**, 11169-11186.
- 45 J. P. Perdew, K. Burke and M. Ernzerhof, *Phys Rev Lett*, 1996, **77**, 3865-3868.
- 46 J. Guan, Z. Zhu and D. Tománek, *Phys Rev Lett*, 2014, **113**, 046804.
- 47 S. Lei, H. Wang, L. Huang, Y.-Y. Sun and S. Zhang, *Nano Lett*, 2016, **16**, 1317-1322.
- 48 D. J. Griffiths, *Introduction to quantum mechanics*, Pearson Educaion, New Jersey, Second edn., 2005.
- 49 C. Buia, A. Buldum and J. P. Lu, *Phys Rev B*, 2003, **67**, 113409.
- 50 C.-P. Lu, G. Li, K. Watanabe, T. Taniguchi and E. Y. Andrei, *Phys Rev Lett*, 2014, **113**, 156804.
- 51 K. H. S. Kirby, D. E. Chris, V. S. Saurabh and P. Eric, *2D Mater*, 2017, **4**, 011009.



Typical structures of two-electrode devices in 2D junction and the corresponding transmission coefficients with the function of bilayer length.